Author Version: *J. Geophys. Res. (C: Oceans), vol.119(10); 2014; 7123–7138.*

Dust-induced episodic phytoplankton blooms in the Arabian Sea during winter monsoon

Priyanka Banerjee and S. Prasanna Kumar*

CSIR-National Institute of Oceanography, Dona Paula, Goa-403 004, India.

*Corresponding author email: prasanna@nio.org

Telephone: 91-832-2450300: Fax: 91-832-2450608

Running Title: Dust-induced phytoplankton blooms

Key Points:

- Mechanistic relation between episodic phytoplankton blooms and dust deposition.
- Importance of atmospheric iron in regions away from active winter convection.
- First report on the inter-annual variability of chlorophyll by dust-derived iron.

Abstract

Phytoplankton blooms mediated by the oceanic supply of nutrients is a well understood phenomenon in the Arabian Sea (AS), while the role of dust deposition in enhancing phytoplankton is less explored. In this paper we show that during winter monsoon the central Arabian Sea (CAS), away from the realm of active winter convection, supports episodic phytoplankton blooms. These blooms cannot be fully explained by the oceanic input of nutrients through processes such as advection and mixing in the upper ocean. Using satellite images we tracked about 45 dust storms over the AS during the winter monsoons of 2002-2003 to 2010-2011 of which only 8 were followed by chlorophyll enhancements. We used a regional climate model to get possible fluxes of dust and the amount of nutrients (nitrate, phosphate and iron) that can be derived from the dust depositions. Additionally, we used published *in situ* nutrients data in conjunction with carbon: nitrogen: phosphorus and iron: carbon molar ratios to compute the potential requirements of different nutrients for the 8 cases of chlorophyll enhancements. It is likely that the deepening of the mixed layer can incorporate nitrate and phosphate, but not enough iron from the subsurface waters leading to potential iron limitation. Although, all the phytoplankton blooms within CAS were observed following episodic dust events, only four blooms can be attributed to dust depositions. Our work shows that phytoplankton blooms fuelled by episodic dust storms are important in driving the inter-annual variability in chlorophyll in a region away from active winter convection.

Keywords: Dust storm, episodic phytoplankton bloom, winter convection, Arabian Sea, dissolved iron, chlorophyll *a* concentration.

1. Introduction

Atmospheric transport of dust aerosols modulates the climate system in numerous ways. One of these is the impact of dust on the primary productivity of the open ocean regions by supplying nutrients, especially micronutrient iron (Fe), leading to drawdown of atmospheric carbon dioxide [*Martin and Fitzwater*, 1988; *Bishop et al*., 2002; *Jickells et al*., 2005; *Gabric et al*., 2010]. The Indian Ocean receives 8 to 32% of the global ocean dust deposition ranging from 29 to 154 Mt/year [*Mahowald et al*., 2005 and references therein]. The Arabian Sea (AS), the northwest part of the Indian Ocean, is the most important sink region for mineral dust coming from South Asia, Southwest Asia and the eastern Horn of Africa [*Prospero et al*., 2002]. Studies show that the highest dust load is in the western and northern AS [example *Li and Ramanathan*, 2002; *Zhu et al*., 2007]. However, these are also the regions where oceanic supply of nutrients (such as nitrate, phosphate and Fe) becomes important through wind-driven coastal upwelling during summer monsoon (SM) in the western AS [*Barber et al*., 2001] and convective mixing during winter monsoon (WM) in the northern AS due to evaporative cooling [*Madhupratap et al*., 1996], making this one of the most productive regions of the world oceans. The mean annual primary productivity in the AS is estimated to be about 111±11mmol C/m^2 /day [*Barber et al*., 2001]. As a comparison, during the spring bloom in the North Atlantic Ocean (47^{o}N, 20^{o}W), the average primary productivity is 90.4±24.1 mmol C/m^2 /day [*Martin et al*., 1993].

Substantial research has been carried out to understand phytoplankton blooms driven by oceanic supply of nutrients in the AS [see for example *Wiggert et al*., 2009 and the references therein]. These studies mainly focused on the supply of macronutrients like nitrate (NO_3) and phosphate (PO_4) through either upwelling or winter convection. On the contrary, the role of dust deposition as a possible mechanism leading to blooms has not been adequately addressed in the AS. The findings of Joint Global Ocean Flux Studies (JGOFS) based on *Measures and Vink* [1999] led *Smith* [2001] to conclude that the AS probably is Fe replete due to high dust deposition. However, a possibility of Fe limitation during the late SM period emerged through the studies of *Wiggert and Murtugudde*, [2007] and *Naqvi et al*., [2010]. Using primarily satellite data few studies have tried to show the effect of dust deposition on phytoplankton from daily [*Singh et al*., 2008] to seasonal [*Patra et al*., 2007] time scales. *Singh et al*. [2008] reported phytoplankton blooms in the northern AS following the passage of individual dust storms for the period December 2003 to December 2006. However, an ambiguity remains regarding the provenance of the nutrients that fuelled these blooms as they also found a decrease in sea surface temperature (SST) due to increased wind mixing during these dust storms. *Patra et al.* [2007] postulated that the region of high

chlorophyll *a* (Chl *a*) during SM coincides with the region having high dust supply rather than the region of strong upwelling. They also concluded that although the eastern AS receives higher oceanic nutrients during WM compared to SM, high Chl *a* is observed during SM compared to WM period because of higher dust supply during SM. An annual increase in Chl *a* in the AS for the time period of 1997-2007 is speculated to be boosted by an increasing mineral dust supply [*Prasanna Kumar et al*., 2010]. Studies also show that only 0.02-0.4% of the Fe in the aerosols over AS is soluble [*Srinivas et al*., 2011] implying very little bioavailability of Fe in dust. *Seifert et al*. [1999] reported less than 4% of Fe in aerosols was soluble and indicated the possibility of atmospheric processing of the Fe. These studies points to the wide range of solubility of Fe present in dust. In the northwest AS for example, where the dust deposition can be around 12 g/m^2/year [*Clemens et al*.,1998], such wide range of Fe solubility results in a wide range of dissolved Fe flux roughly varying between 300 and 15 $\mu mol/m^2$/year. At a greater distance from the dust sources near the southern AS, about 1 g/m^2/year of dust deposition can result in dissolved Fe flux of about 25 to 1 $\mu mol/m^2$/year. A similar notion could be arrived at from extensive studies in other regions of the globe where Fe solubility has been seen to range from 0.01 % to 90% [see Table S3 of *Mahowald et al*., 2005].Thus, the role of dust deposition on the phytoplankton biomass of AS can be highly debatable. It is therefore important to ascertain the extent of contribution of dust to nutrient supply and phytoplankton biomass in this region.

The present study explores the relation between atmospheric dust aerosol and Chl *a* concentrations over the AS using satellite data and modelling. Here we use Chl *a* as a proxy to phytoplankton biomass. Our approach is to analyze if the oceanic supply of nutrients is adequate to support the observed levels of Chl *a* in a region influenced by dust deposition and to provide an estimation of possible nutrients fluxes due to dust depositions. Though episodic dust events occur all through the year, they are more prevalent during SM (June to September), which is a highly productive period due to wind-driven upwelling. Unfortunately, little satellite coverage for SM due to cloud cover prevented us from studying this period. We restrict our study to WM time, defined as encompassing December to March, a period also characterized by high levels of Chl *a* due to entrainment of nutrients by convective cooling and deepening of the mixed layer [*Madhupratap et al*., 1996; *Prasanna Kumar et al*., 2001]. On an average, WM has low dust levels in the atmosphere compared to SM [*Li and Ramanathan*, 2002]. However, episodic dust storms often occur in association with the Shamal weather system [*Perrone*, 1979; *Hubert et al*., 1983] in the surrounding arid landmass. These Shamals are northwesterly winds that blow down the Persian Gulf during both summers and winters. While they are associated with the strength of Indo-

Iranian low during the summer time (June to August), the winter Shamals (November to March) occur following the passage of cold fronts from west to east. They can have wind speed exceeding 20 kilometer/hour and last for 1-2 days and at times up to 5 days. When passing over the arid and semi-arid regions of West and Southwest Asia these disturbances often raise dust that may reach the top of the troposphere.

2. Data and Methods

We used a suite of satellite data and model outputs along with published *in situ* nutrients measurements (N and NO_3, PO_4 and dissolved Fe). The high supply of nutrients through convective mixing makes it important to identify a suitable region that is influenced by episodic dust storms .Using satellite data, we first derived dust optical depth (τ_{du}) and correlated τ_{du} with Chl *a* concentrations to create a correlation map for the AS from which a region having high correlation coefficients was marked out. Next, we investigated the effect of episodic dust storms on the Chl *a* concentrations within the marked region. For the present study the AS domain is defined as 50-78°E longitude and 10-25°N latitude.

2.1. Derivation of dust optical depth

We calculated τ_{du} for the AS from Moderate Resolution Imaging Spectroradiometer (MODIS) onboard Aqua using the method given by *Kaufman et al.* [2005]. Briefly, this is given as:

$$\tau_{du} = [\tau (f_{an} - f) - \tau_{ma} (f_{an} - f_{ma})] / (f_{an} - f_{du}) \ldots\ldots\ldots \text{(i)}$$

For this, monthly mean aerosol optical depth (τ) and fraction of τ contributed by the fine aerosols (f) were obtained from MODIS/Aqua for the period October 2002 to December 2011. $f_{an,}$ f_{ma} and f_{du} are the fine mode fraction of anthropogenic, maritime and dust aerosols respectively. f_{an} was taken as 0.90 based on MODIS measurements in the northern Bay of Bengal (88^o-92^oE, 19^o-21^oN) during WM when anthropogenic fraction dominates the total aerosol load [*Nair et al*., 2005]. f_{ma} was taken as 0.47 based on average value for the period of 2003 to 2011 over the western part of the Equatorial Indian Ocean (55^o-65^oE, 5^o-10^oS) where pristine maritime condition prevails. The standard deviations (SD) for values of f_{an} and f_{ma} were 0.15 and 0.08 respectively. A value of 0.25 was assigned to f_{du} based on satellite values during dust outbreaks in the Middle East. The maritime aerosol optical depth (τ_{ma}) was obtained from the wind speed based equation given by *Smirnov et al.* [2003]:

$$\tau_{ma} = 0.007W\ (m/s) + 0.05\ldots\ldots \text{(ii)}$$

where, W is the wind speed (m/s). Wind data at 10m above the sea surface from QuickSCAT was used during the period 2003 to 2008 followed by ASCAT data (http://cersat.ifremer.fr/data/products/catalogue/) for the remaining years. *Kaufman et al.* [2005] have estimated an error of 10-15% in τ_{du} for $\tau_{du} > 0.1$, while the error in τ is $\pm 0.01 \pm 0.05\tau$ [*Remer et al*., 2002]. Assuming that the error in τ_{du} arises due to the values assigned for f_{an}, f_{du} and f_{ma}, we performed 1000 simulations of τ_{du} using Monte Carlo method [*Geyer*, 2011] and obtained an error of 1.35%.

2.2. Simulation of dust deposition

The Regional Climate Model RegCM 4.0 was employed to simulate the dust deposition, both wet and dry, on 6-hourly basis [*Zakey et al*., 2006]. This type of regional models is best suited for simulating short term events lasting for several days. An on-line dust scheme is included within RegCM 4.0 to calculate emission, transport and deposition of four particle size bins. These bins are 0.01-1 μm, 1-2.5 μm, 2.5-5.0 μm and 5.0-20.0 μm. For the present study simulations over the South and Southwest Asia domain (latitude 10.81°S -46.23°N , longitude 11.28 -113.27°E) were carried out at a spatial resolution of 60 kilometer forced by 6-hourly meteorological fields from NCEP/NCAR reanalysis [*Kalney et al.,* 1996] and land surface data from Biosphere-Atmosphere Transfer Scheme (BATS) [*Dickinson et al*., 1993]. For our present study we compared the simulated τ_{du} with τ_{du} from MODIS/Aqua. Implicit in this comparison is the assumption that a successful simulation of τ_{du} means a proper treatment of emissions and depositions of dust. We have simulated dust depositions for the episodic dust storms to get estimations of possible fluxes of nutrients into the ocean following episodic dust storms.

2.3. Correlation between dust optical depth and chlorophyll concentrations

The τ_{du} so obtained was at 1^o spatial resolution which was averaged for the WM period for each year. Next, monthly mean MODIS/Aqua Standard Mapped Image Chl *a* concentration at 4 kilometer resolution was obtained for the period October 2002 to 2011. The data were regridded to 1^o spatial resolution and a temporal average for the WM for each year was constructed. The τ_{du} and Chl *a* concentrations for the WM of 2002-2003 to 2010-2011 (total 9 years) over the AS were correlated and a correlation map was constructed. This correlation map was used to identify the province over which dust might significantly influence Chl *a* concentrations. However, dust particles suspended in the water can often give a false impression of increased Chl *a* concentrations and can lead to a spurious correlation between dust and Chl *a* [*Claustre et al.,* 2002]. To confirm that the region identified from the correlation

map indeed has high Chl *a*, we constructed a similar map showing correlation coefficient between τ_{du} and MODIS/Aqua Fluorescence Line Height (FLH). FLH was used because only phytoplankton fluoresces in the ocean at 676.6 nm wavelength sensed by MODIS and hence can be effectively used as a proxy for biological activity [*Hu et al.,* 2005; *Lin et al.,* 2011]. By superimposing the correlation contours produced by τ_{du} and FLH with that of τ_{du} and Chl *a* we could identify a region (61-66°E longitude and 11-14°N latitude, designated as central Arabian Sea, CAS; see Section 3.1 for details) having comparatively high values of correlation coefficient of τ_{du} with both the parameters. We used this region (CAS) for further analysis. It is to be noted that although we have used τ_{du} to construct the correlation map, τ_{du} refers to the presence of dust in the atmosphere and not necessarily to dust being actually deposited on the ocean surface. It is actually the dust deposition and associated Chl *a* response which is important. It has been shown by *Schepanski et al*., [2009] in the case of Saharan dust that the relation between optical depth and dust deposition depends on the height at which dust is present. Since continental dust during the WM period travels in the lower levels of the atmosphere due to subsidence [*Krishnamurti et al*., 1998], we expect the value of τ_{du} to reflect the amount being deposited. This has given us confidence in constructing the correlation map using τ_{du} and Chl *a* concentrations. We have restricted the use of model simulated dust depositions only for short term episodic events for which the model is best suited. We have also checked the correspondence between observed and modeled τ_{du} and dust depositions (not shown) and have found broad similarity between the two.

Episodic dust storms during WM which might influence the region marked from the correlation map were identified from NASA Natural Hazards website (http://earthobservatory.nasa.gov/NaturalHazards/) for the abovementioned period. Further, the near real time MODIS imageries (http://rapidfire.sci.gsfc.nasa.gov/realtime) were examined to see the signature of any dust haze over the AS. Time series of 3-day composite Chl *a* concentrations were examined within the outlined region for significant increases in Chl *a* above the background values as well as for the construction of 3-day climatology. The 3-day windows coinciding with the dust storms were discarded to avoid satellite overestimation of Chl *a* concentrations immediately following the dust storms.

2.4. Simulation of mixed layer depth

The state of the water column in the study region was assessed with the help of the mixed layer depth (MLD) data obtained by employing the Price-Weller-Pinkel (PWP) mixed layer model [*Price et al.*,

1986]. PWP is a simple one-dimensional model in which scale analysis suggests that MLD is directly proportional to surface wind stress and inversely proportional to the square-root of surface heat fluxes. The model was initialized with the climatological temperature and salinity profiles from World Ocean Atlas 2009 (WOA09) [*Locarnini et al*., 2010; *Antonov et al*., 2010] and forced by net longwave and shortwave radiation data from NCEP/NCAR reanalysis [*Kalney et al.,* 1996]. Turbulent heat fluxes were obtained from Objectively Analyzed air-sea Fluxes (OAFlux) [*Yu and Weller*, 2007]. Momentum fluxes were calculated from QuickSCAT and ASCAT wind data. For freshwater fluxes (E-P), Evaporation (E) was obtained from OAFlux and Precipitation (P) from Tropical Rainfall Measuring Mission (TRMM) (http://disc.sci.gsfc.nasa.gov/precipitation/tovas/). The daily climatology of the simulated MLD was compared to the MLD derived from *in situ* Argo data (http://www.usgodae.org/cgi-bin/argo_select.pl) using 0.5°C temperature difference criteria.

Additionally, climatology of SST and water column NO_3 and PO_4 distribution were taken from WOA09.

3. Results

3.1. Correlation between dust aerosol and chlorophyll *a* concentration over the Arabian Sea

The annual cycle of τ_{du} and τ is shown in Figure 1a for AS, with highest values during SM and low values in WM for both τ_{du} and τ. This actually reiterates the findings of the earlier studies [example *Li and Ramanathan*, 2002; *Zhu et al*., 2007], which showed that the SM high in τ (> than 0.60) is due to high production of sea salt along with low level transport of dust from the Horn of Africa and mid tropospheric transport from the Arabian Peninsula. It has been estimated that about 30% of τ over the AS is contributed by sea salt [*Satheesh et al*., 2006]. The WM low τ (~0.30) is primarily characterized by low level continental outflow of anthropogenic pollutants [*Lelieveld et al*., 2001] with occasional dust plumes traversing the AS due to events like Shamals. The mean τ_{du} value for the entire AS ranged from 0.44 (SD 0.19) during SM to 0.05 (SD 0.03) during WM.

The τ_{du} showed high positive correlation with both Chl *a* (mean value 0.45) and FLH (mean value 0.40) in the CAS during WM period (Figure 1b), while the patch of high correlation between τ_{du} and Chl *a* extended further north. However, in the north the correlation between τ_{du} and FLH was not very high leading us to conclude that suspended particulate matters probably led to a pseudo correlation. Rest of the AS had little or negative correlation. Though the coastal regions of the AS also showed high positive correlation, for the present study we considered only the open ocean region. Thus, we identify CAS as

the open ocean region (having average depth ~4km) where aeolian dust has the greatest potential of triggering Chl *a* enhancements. However, CAS had comparatively lower value of τ_{du} which was about 0.02 (SD 0.01) (see Figure 1c). In contrast, northern, northeastern and western AS had higher values of τ_{du} but very low or negative correlation coefficient with both Chl *a* and FLH. For instance, the northern AS (NAS, defined as 61-66°E, 20-24°N) had mean τ_{du} of 0.04 (SD 0.01) and correlation coefficient of -0.17. The climatological WM average Chl *a* values in NAS and CAS are about 2.0 mg/m^3 (SD 0.6) and 0.3 mg/m^3 (SD 0.1) respectively (Figure 1c). The maximum Chl *a* values attained at the peak of the bloom based on 3-day mean climatology during WM are ~5.0 mg/m^3 and ~0.4 mg/m^3 respectively. Such a north-south gradient in Chl *a* concentrations can be elucidated by the behavior of the mixed layer (see Figure 1d) which is a proxy for the intensity of winter convection. The magnitude of the deepest mixed layer attained in NAS at the peak of WM (end of January to beginning of February) is more than 100m (deepest MLD from Argo was ~122m). However, the influence of winter mixing, although present, somewhat dwindles towards the south. The deepest Argo-derived MLDs in CAS usually cluster around 80m. Average MLD from Argo during January is 89 m in NAS against 67 m in CAS. Clearly, the deeper penetration of mixing which leads to injection of more nutrients from the subsurface supports the high value of Chl *a* in NAS. The reported NO_3 concentration at the surface is more than 3.0 μM in the NAS in contrast to ~ 2.0 μM NO_3 in CAS [*Madhupratap et al*., 1996; *Morrison et al.,* 1998] (See Section 4.3 for discussion on dissolved Fe). This is further corroborated by Figure 2. The SST increases from 24.5°C in NAS to 26.6°C in CAS, while NO_3 obtained from WOA09, decreases from 2.4 μM in NAS to 0.7 μM in CAS. Note that the NO_3 values from WOA09 are climatological mean for the WM, while the values of *Madhupratap et al*. [1996] and *Morrison et al*., [1998] are spot measurements at the peak of WM of 1995.

3.2. Simulated dust depositions

We next examine the total dust depositions following episodic dust storms. For this model simulated dust deposition (wet+dry) were calculated for episodic dust storms during WM (see Table 1). There were in total 45 dust storms with about 2 to 9 dust storms every year between the WMs of 2002-2003 to 2010-2011 that had the potential of influencing the Chl *a* in the region. These dust storms either sent off plumes over the AS or much less obvious haze (which is more difficult to identify). For brevity, only the result for the 02nd to 05th February, 2008 dust storm is presented as an example (Figure 3). A north to south gradient, similar to that of the distribution of τ_{du} was seen which was common for all other dust

storms (see Supplementary Figure Fs01). The magnitudes, however, showed a large variation from event to event. For example, dust deposition within CAS varied by about an order of magnitude ranging from about 10 mg/m^2 to more than 150 mg/m^2. Spatially the dust deposition decreased significantly from northwest AS towards CAS. Considering Figure 3, the total deposition during the dust storm of 02nd to 05th February, 2008 was one order of magnitude higher in NAS (~ 1300 mg/m^2) compared to CAS (~100 mg/m^2). Comparing the values with those derived from sediment trap, dust depositions ranges from about 33 mg/m^2/day at around 17° N to 4 mg/m^2/day at 10° N[*Clemens*, 1998]. The predominant (more than 90%) size fraction of the deposited dust in CAS were between 0.01 and 1 μm (fine mode fraction).Most of the medium to small-sized events were responsible for wet depositions which varied between 0.1 to 72 % (see Table 1). This has important implications for the bio-availability of Fe as cloud processing of the Fe during wet processes increases the solubility of Fe [see example *Duce and Tindale*, 1991].

A comparison of the model simulated τ_{du} with that of remotely sensed data from MODIS/Aqua showed that while the model could successfully reproduce the spatial and temporal pattern of τ_{du}, there is general underestimation with respect to dust storms which have values of τ_{du} that are well above 1(Figure 3). The extent of underestimation becomes larger towards the southern part of AS. However, in the immediate vicinity of the dust sources the model overestimates. It is important to note that satellite measured τ_{du} captures a snapshot of aerosol each day, while the model is forced by 6-hourly wind. Nonetheless, the underestimations in τ_{du} for some of the highest dust storms are expected to reflect in the dust depositions and the calculations of the possible amount of nutrients that can be derived from dust.

3.3. Enhancements of chlorophyll *a* following episodic dust storms in the central Arabian Sea

During the time period under study, 8 episodes of Chl *a* enhancements following the passage of dust storms were discerned (Figure 4) when the average Chl *a* enhanced 2 to 4 times the background values in CAS. The criterion chosen to identify the Chl *a* enhancements was that it should be more than 2 SD of the climatological values. These 8 cases were further segregated according to different phases of the mixed layer evolution (Figure 5 and Table 2). The Chl *a* enhancements during E1 (episode 1) was associated with mature phase of winter convection. E4 and E5 were in the early part of winter convection when the mixed layer was in the deepening phase as inferred from the PWP model.

Conversely, the Chl *a* enhancements during E1, E3, E6 and E7 were associated with the shallowing phase of the winter convection. The high Chl *a* episode during E8 took place following the cessation of winter convection when MLD was around 22 m.

4. Discussions

4.1 Possible mechanisms leading to phytoplankton blooms in the CAS

The pattern of nutrients supply to the AS is primarily governed by the physical processes that control the degree of mixing in the upper layer of the ocean. A deeper mixed layer, as encountered in the NAS, is conducive for supplying higher subsurface nutrients and therefore higher Chl *a* concentrations. A comparatively shallow mixed layer towards the south leads to decreased nutrients supply which is responsible for the lower levels of Chl *a*. It is this set-up which makes CAS a suitable region for detecting the dust induced Chl *a* enhancements. Although dust depositions are expected to have effect on the nutrient stocks within NAS, its effects are largely masked by the huge water column turn-over of nutrients. Dust is more efficient in feeding the phytoplankton stocks in the regions experiencing limited oceanic supply of nutrients. Thus, a low dust flux can have its imprint on the CAS phytoplankton biomass. The region south of CAS has too little oceanic nutrient inventories and/or is too remote from dust sources to have appreciable Chl *a* levels during WM. So, it is the crucial location of CAS, which hinges on the balance between oceanic nutrients supply and atmospheric depositions, that resulted in the positive correlation between dust optical depth and Chl *a*.

There were in total 8 cases of episodic Chl *a* enhancements following passage of dust storms within CAS. However, we have to be cautious in determining whether the enhancements can indeed be attributed to atmospheric depositions. In general, three factors could lead to the Chl *a* enhancements in the CAS during WM: (1) advection of nutrients and/or Chl *a* from a region of high production, (2) wind-mixing and/or winter convection and subsequent entrainment of nutrients to the upper ocean and (3) atmospheric deposition of nutrients. Over the CAS, the prevailing ocean surface current at this time of the year is weak (~0.1 m/s) and the general direction is from south to north as inferred from Figure 1c, which is not congenial for the advection of nutrients into this region. The same direction was maintained during each of these studied episodes with some changes in magnitudes. Since the region south of CAS is low in Chl *a* and nutrients, advection as a mechanism to support the observed high Chl *a* in CAS can be discounted.

Next, we consider the case of wind-mixing and/or winter convection as potential source of nutrients to the upper ocean by examining the modeled MLD (Figure 4 and Table 1). Dust storms are generally associated with high wind speed (more than 10 m/s) that can lead to greater mixing of the upper water column. Indeed, 3 out of the 8 dust storms (E1, E3 and E6) had wind speed greater than 10 m/s. Also the deepening of the mixed layer associated with winter convection leads to gradual build up of nutrients within this layer (see also Figure 2), which can potentially support the observed Chl *a* levels. An important observation in this regard is that under dust-storm free conditions MLD has been seen to deepen (due to winter convection or high winds) without any appreciable enhancement (not presented) of Chl *a* indicating that MLD deepening alone cannot mitigate the nutrient(s) limitation in CAS. In view of the above discussion we first try to estimate the requirements of different nutrients (total inorganic N, PO_4 and dissolved Fe) for the observed enhancements of Chl *a* concentration and compare the demand to the supply of these nutrients.

4.2 Requirements versus supply of nitrate and phosphate

Table 2 shows the requirements of total inorganic N, PO_4 and dissolved Fe for the observed levels of Chl *a* enhancements following dust storms. For calculating requirements of N and PO_4 we have assumed that carbon: nitrogen: phosphorus (C: N: P) ratio of 106:16:1 [*Redfield et al*., 1963] and C/Chl *a* (μg carbon/μg Chl *a*) ratio of 186 obtained from *in situ* measurements in the AS [*Takeda et al.,* 1995]. If we compare the values obtained in Table 2 with the available nutrients data during JGOFS, we see that at the peak of WM the surface NO_3 values within CAS ranges between ~1.0 to 3.0 μM with an average of ~2.0 μM while the total inorganic Nitrogen (NO_3+NO_2+NH_4) can be well above 3.5 μM [*Morrison et al.,* 1998]. *Madhupratap et al.* [1996] found surface NO_3 less than 2.0 μM. Similarly during JGOFS PO_4 has been seen to vary between 0.3 and 0.5 μM within CAS [*Morrison et al.,* 1998]. We see that requirements versus the oceanic supply of inorganic N and PO_4 are in the same order of magnitude given the uncertainties involved and hence we can conclude that inorganic N and PO_4 were likely not limiting at the time of the dust storms. Although levels of nutrients residing in the mixed layer can vary from year to year, several studies [example *Prasanna Kumar et al*., 2001] have shown that it is the depth of mixing dictated by the intensity of winter convection that exerts the first order influence on the replenishment of nutrients. We have carefully compared the MLD and SST during the times when inorganic N and PO_4 data were retrieved with the present episodes (not shown) and have come to the conclusion that there is broad similarity in the intensity of winter convection between these years.

An examination of the dust sample collected on 10th April 2013 using high volume sampler at a station in Goa, along the west coast of India, during a dust storm event yielded a NO_3 concentration of ~20 mg/ g of dust (V. Ramaswamy personal communications). Note that Milli-Q water was used to extract NO_3 from dust. This when compared to the dust depositions and the depth of mixing within the water column gives an insignificant increase in NO_3. This is in agreement with the conclusion drawn by *Singh et al*. [2012] regarding dust aerosol being a limited source of nitrogen and contributing to just 1.2 % of the new production in the AS during WM. However, in the case of E7, the requirement of N (~5 μM) at the peak of the bloom significantly exceeds that of the estimated instantaneous oceanic supply, indicating that the requirement was likely met from N build up during initial stage of the bloom when the phytoplankton biomass was comparatively low. Similarly, PO_4 concentration was about 0.2 mg/g of dust, which also results in negligible contribution to the water column. Thus, based on the climatological concentrations of inorganic N (including NO_3) and PO_4 in the water column and the amount of new nutrients that can be derived from dust, we conclude that the main source of N and PO_4 for these episodes of phytoplankton blooms is the water column. In fact, the climatological concentrations of inorganic N and PO_4 at the peak of WM should be able to support Chl *a* levels of ~1.0 mg/m^3. Since, climatological Chl *a* concentration is about 0.4 mg/m^3; it implies that some other nutrient must be missing.

4.3. Requirements versus supply of dissolved iron

It is clear from the previous section that the supply of a nutrient other than N and PO_4 must have played an important role in episodically enhancing the phytoplankton stocks. Because dust is an important source of Fe it brings forth an interesting possibility that the region might be experiencing some Fe limitation and Fe from episodic dust storms might be leading to the observed episodic Chl *a* enhancements. The main function of iron in the phytoplankton is its role as a catalyst in photosynthesis [*Geider and La Roche*, 1994]. In Fe limited environments, an increase in the external supply of dissolved Fe (DFe) will lead to enhanced DFe uptake and specific growth rate. For example, for the oceanic diatom *Thalassiosira oceanica*, an increase in external DFe from 10.6 to 760 pM increases Fe/C ratio (μmol/mol) from 4.9 to 33.9 [*Sunda and Huntsman,* 1995]. We have considered a range of cell Fe/C ratios to study the DFe requirements under different conditions of availability of DFe and the implied sensitivities: (1) A mean value of 7.5 over the AS based on modelling by *Moore et al.*[2002], (2) based on apparent oxygen utilization, *Sunda* [1997] arrived at a Fe/C ratio of 12.8 for North Atlantic Ocean during the spring bloom time when primary productivity ranges from 71.3 to 91.1 mmol C/m^2

/day [*Martin et al*., 1993] and (3) a ratio of 33.9 indicator of the highest possible DFe requirements based on laboratory experiments [*Sunda and Huntsman,* 1995]. Based on the above 3 cell Fe/C ratios (namely 7.5, 12.8 and 33.9) the results for the calculation of DFe requirements are shown in Table 2.

Much care is needed in order to ascertain the supply side of DFe. Few sets of *in situ* DFe (defined as Fe that can pass through 0.2 μm filter) measurements exist in the AS during the WM: (1) surface sampling along 65°E meridional transect and a profile at 15°N by *Takeda et al.* [1995] during end of December, 1992 to beginning of January, 1993 (2) along US JGOFS track by *Measures and Vink* [1999] during January-February, 1995 as a part of US JGOFS Arabian Sea Process Studies and (3) recently, as a part of the GEOTRACES program, DFe was measured roughly along 69°E, to the east of the present study region during the WM of 2009 [*Nishioka et al*., 2013; *Vu and Sohrin*, 2013]. Two important observations emerge from these studies: (1) a general increase in the DFe concentrations from south to north and (2) within CAS, the ferricline lies at a depth deeper than the nitracline with the difference between the two about 25m. So while the MLD attained at the peak of the WM can erode the top of the nitracline, it may not be able to erode the top of the ferricline within CAS. However, within NAS, both nitracline and ferricline can be eroded by the deep mixing under winter convection. This mismatch between the depth of nitracline and ferricline probably has the potential of turning CAS into a Fe-limited region. Being surrounded by dust sources AS receives mineral dust flux throughout the year. Hence, we first need to ascertain just the oceanic supply of DFe to see whether the episodic Chl *a* enhancements in CAS can be supported by DFe supplied from the water column alone. For this we calculated the entrainment of DFe with the progress of WM using the profile of *Takeda et al*. [1995] with the assumption that the values reflect the ambient concentrations. This enables us to account for the entrainment of DFe with the deepening of mixed layer. The rationale for our assumption is that the DFe values of *Takeda et al*. [1995] is measured earlier in the WM period compared to *Measures and Vink* [1999] and the values are significantly lower (mean DFe ~ 0.3 nM) compared to those collected by the latter (~1nM). While there are several uncertainties associated with this method, in the absence of more *in situ* DFe measurements, we believe that this shall be a convenient starting point to understand how oceanic DFe supply is regulated.

The surface DFe values measured by *Takeda et al*. [1995] ranges between 0.15 nM (at 12°30'N lying within CAS) to 0.47 nM (at 17°30'N) and at 15°N it is 0.23 nM. The MLD during the study by *Takeda et al.* [1995] at 15°N was around 50m. With the progress of WM, the deepening of MLD to about 80m within CAS entrains DFe to the surface waters. We estimated that for a 80m deep MLD, winter

entrainment process results in the mixed layer DFe concentration of about 0.33 nM. This value matches with those from GEOTRACES cruise data collected to the east of the study region with reported value of DFe of 0.35 nM and MLD of around 70m. We expect the available DFe within CAS to be lower than the above calculated value since the region is situated more south of the location where the DFe profile was collected. The surface DFe value within CAS is almost 1.5 times less than the surface DFe value at 15°N where the DFe profile has been taken. Accordingly, if we scale the DFe value obtained due to winter entrainment at 15°N, the DFe within CAS due to winter entrainment comes to ~0.2 nM. On comparing this value with the DFe requirements estimated from the Fe/C ratios (Table 2), we see that at Fe/C ratio of 7.5 the entire requirements can be met from the water column for all the cases of Chl *a* enhancements except E7. However, as the Fe/C ratio shifts to higher values, the water column DFe supply becomes increasingly insufficient. For Fe/C ratio of 12.8, episodes E1, E2, E4, E6 and E7 would require an external source of DFe. At Fe/C ratio 33.9, all of the episodic phytoplankton blooms would require external DFe. However, the ratio of 33.9 (mainly applicable for diatoms) is only a theoretical assumption in this case and is highly unlikely as CAS is primarily dominated by Picoplankton (see Section 4.4).

Next, we consider an aeolian source of DFe. We have assumed about 3.5% Fe content in the soil dust [*Taylor and McLennan*, 1985]. Dust deposition within CAS is primarily dominated by fine mode fraction (see Section 3.2). Upon being deposited on the ocean surface a certain fraction of Fe in the dust is instantaneously dissolved followed by a much longer time dissolution of Fe (ranging from hours to weeks) [*Mackie et al*., 2006; *Boyd et al*., 2010]. It has been reported that during May when air masses over the AS comes mainly from the Middle East, thereby enriched with crustal materials, the fraction of labile Fe (II) to total Fe in the fine mode fraction of the aerosol (< 3.0 μm) varies from less than 1% to around 8% [*Seifert et al*., 1999]. This includes both the instantaneous and the long term soluble Fe fraction. It has also been seen that with increasing distance from land the fraction of labile Fe (II) in the total aerosol can be ~50% [example *Zhuang et al*., 1992]. By considering DFe constituting 1% ($DFe_{1\%}$), 10% ($DFe_{10\%}$) and 50% ($DFe_{50\%}$) of the total Fe in dust we have calculated the probable ranges of atmospheric supply of DFe during these episodic events. Based on this, Table 1 shows the total amounts of DFe that can be extracted following dust depositions. Note, at this point that we have noticed considerable underestimation of τ_{du} for episodes E1, E6 and E7 (where the τ_{du} value exceed 1) which will impact the dust deposited and the amount of DFe that can be possibly derived. A comparison of the possible scenarios when total DFe (dust-derived + oceanic supply) can meet the Chl *a* requirements is

depicted in the form of a matrix in Figure 6. Maximum cases of Chl *a* enhancements are supported at Fe/C ratio of 12.8 along with $DFe_{10\%}$ and $DFe_{50\%}$ (a scenario that is not quite likely). At Fe/C ratio of 7.5, demand for DFe is entirely met from the water column inventory, while at the extreme Fe/C ratio of 33.9 the demand for DFe is too high even at $DFe_{50\%}$ (an extreme that is also highly unlikely). It is quite possible that Chl *a* during E7 and E8 are likely to draw DFe not only from the immediate dust storm event, but also from previous events as there were continuous pulses of dust depositions during this year (that is, 2008) which would lead to slow build up of DFe within the surface mixed layer. In case of the dust deposition events which are accompanied by significant wet depositions (E1, E3, E4 and E6), the likelihood of bio-availability of Fe increases even for small deposition fluxes. Based on the above calculations (and Figure 6) that highlight the different requirement versus supply scenarios, we conclude that the phytoplankton blooms related to episodes E1, E4, E6 and E7 are likely fuelled by dust derived DFe when the Fe/C ratio is 12.8 and about 10% of Fe in dust is dissolved ($DFe_{10\%}$). For episode E2, although the requirement of DFe cannot be met by the water column, our calculation implies that dust can support the bloom provided the fraction of Fe that is soluble in dust is much greater than 10%. This in its entirety is conceptualized in Figure 7 which shows how the degree of oceanic mixing sets the stage for atmospheric deposition to alter the biogeochemistry of the region. Following addition of DFe during dust storms there can be multiplication of large sized phytoplankton leading to a bloom condition.

The episodic Chl *a* enhancements took place after a time lag which varied from 1 to 10 days following the passage of the dust storms (see Table 1 and 2) and 20 days in case of E3. It is important to note that once a dust-storm is detected by a satellite it may take a day or two or at time up to five days for the storm to travel to CAS. Time lags of 1-2 days [*Singh et al.*, 2008] to 5-6 days [*Bishop et al.*, 2002] have been reported elsewhere. The observed magnitude and timing of Chl *a* enhancements following the dust storms should match with the time required for Fe dissolution plus the time required for phytoplankton growth to take place. The time scale for dissolution of Fe ranges from hours to weeks depending on the mechanism involved [see *Boyd et al*., 2010 and references therein]. For example, dissolution of Fe by photolysis of colloidal ferrihydrite takes hours [*Barbeau and Moffett*, 2000]; while flagellate mediated phagotrophy can solubilize Fe within a time period of 2 to 10 days [*Nodwell and Price*, 2001].

Thus, from the above discussion it is evident that the possibility of an atmospheric supply driving the episodic blooms depends on the amount of DFe that can be extracted from the dust depositions and the assumed Fe/C ratios. Although CAS shows a positive correlation between τ_{du} and Chl *a*, dust

depositions actually leading to phytoplankton blooms has to be dealt with caution as several factors like amount of dust deposition, DFe that can actually be extracted, the MLD and availability of other nutrients come into play. However, the important point remains that although all dust storms are not followed by phytoplankton blooms, these blooms are detected only following dust storms. In the absence of dust storms, even high winds do not lead to blooms indicating nutrient deficiency in the system. This probably arises because the top of the nitracline is shallower than the ferricline. The estimates of dust-derived DFe given by us are only indicative. With the availability of more DFe data from this region, the ranges of DFe that can be supplied by dust can be narrowed down.

4.4 Significance of dust deposition related to community structure of the Arabian Sea

The AS undergoes a steady transition from a stratified oligotrophic system to a highly productive system in the north characterized by deep mixing with the onset of WM. Such transition is usually accompanied by community succession: from Picoautotrophs to larger size Microautotrophs, especially Diatoms and Dinoflagellates [*Garrison et al*., 2000]. However, southwards, within the nutrient-depleted CAS the autotrophic biomass is mainly dominated by Picoplankton followed by Nanoplankton [*Garrison et al*., 2000]. This north-south distinction in the autotrophic community is also reflected in the grazers consisting of mainly heterotrophic bacteria indicative of microbial food web within CAS. In contrast, Mesozooplankton makes up much of the food web in the productive parts of AS [*Smith and Madhupratap*, 2005]. Without any nutrient addition the growth rate (~0.4/day) of the autotrophs within CAS matches the grazing rate (~0.5/day) [*Landry et al*., 1998]. It has been estimated that grazing accounts for consumption of 29% of the Chl *a* [*Caron and Dennett*, 1999] within the CAS region. If this amount is added to the levels of Chl *a* sensed by satellites, then the actual requirement for nutrients become even larger. *Takeda et al*. [1995] has demonstrated that phytoplankton in AS achieved a mean growth rate of 0.6/day following addition of NO_3 and Fe, in spite of not screening out the grazers. The increase in phytoplankton biomass in their experiment was accompanied by predominance of diatoms leading to the conclusion that phytoplankton growth is co-limited by NO_3 and Fe**,** at least in the initial stage of winter monsoon. However, as the winter convection intensifies with time, the nitrate builds up within the mixed layer. Eventually, the phytoplankton growth may be limited by Fe and an adequate atmospheric deposition of DFe can possibly relieve them of Fe stress. It is worth mentioning that the contribution of new Fe to total Fe supply varies from 10% in high-nutrient-low-chlorophyll (HNLC) waters to 50% in Fe-replete waters [see *Boyd and Ellwood*, 2010 and references therein]. As the NO_3 + Fe addition leads to increased Chl *a*, other nutrients like P and Si becomes limiting. Such a shift in the

community with the addition of NO_3 + Fe has important implications for carbon export as this seemingly expands the domain of winter convection much more southwards.

4.5. Contribution of dust to inter-annual variability in the chlorophyll *a*

The incidences of Chl *a* enhancements following the passage of dust storms led us to investigate how far are the episodic events important in defining the inter-annual variability of Chl *a* over CAS during WM? Figure 8a clearly depicts the difference between phytoplankton biomass during the WMs of the three years having highest τ_{du} (2003-2004, 2006-2007 and 2007-2008) and rest of the six years with low τ_{du} (Figure 8b). The WMs of these three years together contributed to 46.6% of the total Chl *a* concentration within CAS when all the nine years of the study period are considered. The WMs of 2003-2004 and 2007-2008 alone contributed to 38.5% of Chl *a* within CAS. The two years with the highest values of τ_{du} were the WMs of 2003-2004 (τ_{du} of 0.04) and 2007-2008 (~0.05). These two years had average Chl *a* of 0.83 mg/m^3 and 0.57 mg/m^3 respectively. In contrast, the years with lower levels of dustiness had average Chl *a* of 0.31 mg/m^3. For the three years with the highest τ_{du} (2003-2004, 2006-2007 and 2007-2008), CAS accounted for about 43.0% of the total Chl *a* of the AS (60-67°E, 5-25°N) during WM period. For the rest of the six years CAS accounted for only 24.3% of the total Chl *a* of the entire AS for the WMs. It is therefore evident that, although, CAS supports low levels of Chl *a* biomass during the WM time, the influence of episodic events like dust depositions supplying DFe can turn CAS into a productive system and account for a large part of the inter-annual variability within this region.

5. Conclusion

The AS has high levels of Chl *a* due to oceanic nutrients supply driven by winter convection during the WM. Added to this the high dust deposition makes this region a suitable natural laboratory to study the dynamical interactions between phytoplankton and different modes of supply of nutrients. While NAS has high dust deposition, its immediate impact on the Chl *a* is masked due to high oceanic nutrients (inorganic N, PO_4 and DFe) supply through convective mixing. At the other end of the spectrum, although dust deposition is attenuated at CAS, its role in nourishing the phytoplankton stocks is conspicuous because of limited oceanic DFe supply. The unique location of CAS, at the periphery of the AS winter convection region leads to incorporation of NO_3 from the top of the nitracline, but probably not DFe from the top of the ferricline which is deeper. With the input of dust, if sufficient quantities of DFe are bio-available, episodic blooms can be observed as reported in the study. However, attribution of

such blooms to dust depositions has to be done with care. Based on the limited available data for our study period, only 4 cases of episodic Chl *a* enhancements (E1, E4, E6 and E7) can be attributed to mineral dust. The rest of the cases depend on the sensitivity to the amount of DFe that can be extracted from dust deposited (both wet and dry). Such episodic events, though not ubiquitous, are significant to drive inter-annual variability in the Chl *a* of the AS which has not been hither to credited.

Our present work is based on satellite observations and *in situ* measurements obtained from published literature. Clearly, more collocated measurements are required to be able to better comprehend the relation between dust depositions and the phytoplankton bloom. This has regional as well as global implications especially with respect to CO_2 budget in a changing climate scenario.

Acknowledgments

The authors thank the Director CSIR-NIO Goa and Council of Scientific and Industrial Research (CSIR), New Delhi for all support and encouragement. We are grateful to Kenneth Coale and an anonymous reviewer for the excellent review that has helped us immensely to improve the manuscript. We also thank V. Ramaswamy, Chief Scientist, CSIR-NIO for discussions regarding the composition of dust collected over Goa, India. This forms a part of the "Mineral dust fluxes and impact on ocean and coastal ecosystem" under GEOSINKS program funded by CSIR. Ms. Banerjee acknowledges CSIR for Senior Research Fellowship. This is NIO contribution XXXX.

References

Antonov, J. I., D. Seidov, T. P. Boyer, R. A. Locarnini, A. V. Mishonov, H. E. Garcia, O. K. Baranova, M. M. Zweng, and D. R. Johnson (2010), *World Ocean Atlas 2009*, vol. 2, Salinity, edited by S. Levitus, 184 pp., U.S. Govt. Print. Off., Washington, *D. C.*

Barber, R. T., J. Marra, R. C. Bidigare, L. A. Codispoti, D. Halpern, Z. Johnson, M. Latasa, R. Goericke, and S. L. Smith (2001), Primary productivity and its regulation in the Arabian Sea during 1995, *Deep Sea Res., Part II*, 48, 1127–1172.

Barbeau, K., *and* J. W. Moffett (2000), Laboratory and field studies of colloidal iron oxide dissolution as mediated by phagotrophy and photolysis, *Limnol. Oceanogr.*, 45, 827–835.

Bishop, J. K. B., R. E. Davis, and J. T. Sherman (2002), Robotic observations on dust storm enhancement of carbon biomass in the North Pacific, *Science*, 298, 817–821.

Boyd, P. W., and M. J. Ellwood (2010), The biogeochemical cycle of iron in the ocean, *Nat. Geosci*., 3, 675–682, doi:10.1038/ngeo964 .

Boyd, P. W., D. S. Mackie, and K. A. Hunter (2010), Aerosol iron deposition to the surface ocean—Modes of iron supply and biological responses, *Mar. Chem.*, 120, 128–143, doi:10.1016/j.marchem.2009.01.008.

Caron, D. A., and M.R. Dennett (1999), Phytoplankton growth and mortality during the 1995 northeast monsoon and spring intermonsoon in the Arabian Sea, *Deep Sea Res., Part II*, 46,1665–1690.

Claustre, H., A. Morel, S. B. Hooker, M. Babin, D. Antoine, K. Oubelkheir, A. Bricaud, K. Leblanc, B. Quéguiner, and S. Maritorena (2002), Is desert dust making oligotrophic waters greener? *Geophys. Res. Lett.*, 29(10), 1469, doi:10.1029/2001GL014056.

Clemens, S. C. (1998), Dust response to seasonal atmospheric forcing: Proxy evaluation and calibration, *Paleoceanography*, 13, 471–490, doi:10.1029/98PA02131.

Dickinson, R.E., A. Henderson-Sellers, and P.J. Kennedy (1993), Biosphere-atmosphere Transfer Scheme (BATS) Version 1e as Coupled to the NCAR Community Climate Model. NCAR Technical Note NCAR/TN-387+STR, doi: 10.5065/D67W6959.

Duce, R.A., and N. W. Tindale (1991), The atmospheric transport of iron and its deposition in the ocean, *Limnol. Oceanogr*., 36, 1715– 1726.

Gabric, A. J., R. A. Cropp, G. H. McTainsh, B. M. Johnston, H. Butler, B. Tilbrook, and M. Keywood (2010), Australian dust storms in 2002–2003 and their impact on Southern Ocean biogeochemistry, *Global Biogeochem. Cycles*, 24,GB2005, doi:10.1029/2009GB003541.

Garrison, D. L., et al. (2000), Microbial food web structure in the Arabian Sea: A U.S. JGOFS study, *Deep Sea Res., Part II*, 47, 1387–1422.

Geider, R. J., *and* J. La Roche (1994), The role of iron in phytoplankton photosynthesis, and the potential for iron-limitation of primary productivity in the sea, *Photosynth. Res.*, 39(3), 275–301, doi:10.1007/BF00014588.

Geyer, C. J. (2011) Introduction to Markov Chain Monte Carlo. In *Handbook of Markov chain Monte Carlo.* (eds S. Brooks, A. Gelman, G. K. Jones and Meng X. L.) FL: CRC Press. pp. 3–48.

Hu, C., F. E. Muller‐Karger, C. Taylor, K. L. Carder, C. Kelble, E. Johns, and C. A. Heil (2005), Red tide detection and tracing using MODIS fluorescence data: A regional example in SW Florida coastal waters, *Remote Sens. Environ.*, 97, 311‐321, doi:10.1016/j.rse.2005.05.013.

Hubert, W. E., D. R. Morford, A. N. Hull, and R. E. Englebretson (1983), Forecasters handbook for the Middle East/Arabian sea, Rep. CR 83-06, Nav. Environ. Predict. Res. Facil., Monterey, Calif.

Jickells, T. D., et al. (2005), Global iron connections between desert dust, ocean biogeochemistry, and climate, *Science*, 308, 67–71, doi:10.1126/science.1105959.

Kalnay, E., et al. (1996), The NCEP/NCAR 40-year reanalysis project, *Bull. Am. Meteorol. Soc*., 77, 437–471.

Kaufman, Y., I. Koren, L. A. Remer, D. Tanre, P. Ginoux, and S. Fan (2005), Dust transport and deposition observed from the Terra-MODIS spacecraft over the Atlantic Ocean, *J. Geophys. Res*., 110, D10S12, doi:10.1029/2003JD004436.

Krishnamurti, T. N., B. Jha, J. Prospero, A. Jayaraman, and V. Ramanathan (1998), Aerosol and pollutant transport and their impact on radiative forcing over the tropical Indian Ocean during the January–February 1996 pre-INDOEX cruise, *Tellus, Ser. B*, 50, 521–542.

Landry, J. R., S. L. Brown, L. Campbell, J. Constantinou, and H. Liu, Spatial patterns in phytoplankton growth and microzooplankton grazing in the Arabian Sea during monsoon forcing (1998), *Deep Sea Res., Part II*, 45, 2353–2368.

Lelieveld, J., et al. (2001), The Indian Ocean Experiment: Widespread air pollution from south and southeast Asia, *Science*, 291, 1031–1036, doi:10.1126/science.1057103.

Li, F., and V. Ramanathan (2002), Winter to summer monsoon variation of aerosol optical depth over the tropical Indian Ocean, *J. Geophys. Res*., 107(D16), 4284, doi:10.1029/2001JD000949.

Lin, I.-I., et al. (2011), Fertilization potential of volcanic dust in the low-nutrient low-chlorophyll western North Pacific subtropical gyre: Satellite evidence and laboratory study, *Global Biogeochem. Cycles*, 25, GB1006, doi:10.1029/2009GB003758.

Locarnini, R. A., A. V. Mishonov, J. I. Antonov, T. P. Boyer, H. E. Garcia, O. K. Baranova, M. M. Zweng, and D. R. Johnson (2010), *World Ocean Atlas 2009*, vol. 1, Temperature, edited by S. Levitus, 184 pp., U.S. Govt. Print. Off., Washington, D. C.

Mackie, D. S., J. M. Peat, G. H. McTainsh, P. W. Boyd, *and* K. A. Hunter *(*2006*),* Soil abrasion and eolian dust production: Implications for iron partitioning and solubility, *Geochem. Geophys. Geosyst*., *7*, Q12Q03, doi:10.1029/2006GC001404.

Madhupratap, M., S. Prasanna Kumar, P. M. A. Bhattathiri et al. (1996), Mechanism of the biological response to winter cooling in the northeastern Arabian Sea, *Nature*, 384, 549–552.

Mahowald, N., A. Baker, G. Bergametti, N. Brooks, R. Duce, T. Jickells, N. Kubilay, J. Prospero, and I. Tegen (2005), The atmospheric global dust cycle and iron inputs to the ocean, *Global Biogeochem. Cycles*, 19, GB4025, doi:10.1029/2004GB002402.

Martin, J. H., and S. Fitzwater (1988), Iron deficiency limits phytoplankton growth in the northeast pacific subarctic, *Nature*, 331, 341–343, doi:10.1038/331341a0.

Martin, J., S. Fitzwater, R. Gordon, C. Hunter, and S. Tanner (1993), Iron, primary production and carbon-nitrogen flux studies during the JGOFS North Atlantic Bloom Experiment, *Deep Sea Res., Part II*, 40, 115–134.

Measures, C.I., and S. Vink (1999), Seasonal variations in the distribution of Fe and Al in the surface waters of the Arabian Sea, *Deep Sea Res., Part II*, 46,1597-1622.

Moore, J. K., S. C. Doney, D. M. Glover, and I. Y. Fung (2002), Iron cycling and nutrient-limitation patterns in surface waters of the world ocean, *Deep Sea Res., Part II*, 49, 463–507.

Morrison, J. M., L. A. Codispoti, S. Gaurin, B. Jones, V. Manghnani, and Z. Zheng (1998), Seasonal variation of hydrographic and nutrient fields during the US JGOFS Arabian Sea Process Study, *Deep Sea Res., Part II,* 45, 2053–2101.

Nair, S. K., K. Parameswaran, and K. Rajeev (2005), Seven-years satellite observations of the mean structure and variabilities in the regional aerosol distribution over the oceanic areas around the Indian subcontinent, *Ann. Geophys*., 23, 2011–2030.

Naqvi, S.W.A., et al. (2010), The Arabian Sea as a high-nutrient low-chlorophyll region during the late Southwest Monsoon, *Biogeosciences*, 7, 2091–2100, doi: 10.5194/bg-7-2091-2010.

Nishioka, J., H. Obata, and D. Tsumune (2013), Evidence of an extensive spread of hydrothermal dissolved iron in the Indian Ocean, *Earth Planet. Sc. Lett*., 361, 26–33.

Nodwell, L. M., and N. M. Price (2001), Direct use of inorganic colloidal iron by marine mixotrophic phytoplankton, *Limnol. Oceanogr*., 46(4), 765–777.

Patra, P. K., M. D. Kumar, N. Mahowald, and V. V. S. S. Sarma (2007), Atmospheric deposition and surface stratification as controls of contrasting chlorophyll abundance in the North Indian Ocean, *J. Geophys. Res*., 112, C05029, doi:10.1029/2006JC003885.

Perrone, T. J. (1979), Winter Shamal in the Persian Gulf, Tech. Rep. TR 79-06, 168 pp., Nav. Environ. Predict. Res. Facil., Monterey, Calif.

Prasanna Kumar, S., N. Ramaiah, M. Gauns, V. V. S. S. Sarma, P. M. Muraleedharan, S. Raghukumar, M. D. Kumar, and M. Madhupratap (2001), Physical forcing of biological productivity in the northern Arabian Sea during the Northeast Monsoon, *Deep Sea Res., Part II*, 48(6–7), 1115–1126, doi:10.1016/S0967-0645(00)00133-8.

Prasanna Kumar, S., R. P. Roshin, J. Narvekar, P. K. Dinesh Kumar, and E. Vivekanandan (2010), What drives the increased phytoplankton biomass in the Arabian Sea?, *Curr. Sci*., 99, 101–106.

Price, J. F., R. A. Weller, and R. Pinkel (1986), Diurnal cycling: Observations and models of the upper ocean response to diurnal heating, cooling, and wind mixing, *J. Geophys. Res*., 91(C7), 8411–8427, doi:10.1029/JC091iC07p08411.

Prospero, J. M., P. Ginoux, O. Torres, S. E. Nicholson, and T. E. Gill (2002), Environmental characterization of global sources of atmospheric soil dust identified with the NIMBUS 7 TOMS absorbing aerosol product, *Rev. Geophys*., 40(1), 1002, doi:10.1029/2000RG000095.

Redfield, A. C., B. H. Ketchum, and F. A. Richards (1963), The influence of organisms on the composition of seawater, in *The Sea*, vol. II, edited by M. N. Hill, pp. 26–77, Interscience, New York.

Remer, L. A., et al. (2002), Validation of MODIS aerosol retrieval over ocean, *Geophys. Res. Lett*., 29(12), 8008, doi:10.1029/2001GL013204.

Satheesh, S. K., J. Srinivasan, and K. K. Moorthy (2006), Contribution of sea-salt to aerosol optical depth over the Arabian Sea derived from MODIS observations, *Geophys. Res. Lett*., 33, L03809, doi:10.1029/2005GL024856.

Schepanski, K., I. Tegen, and A. Macke (2009), Saharan dust transport and deposition towards the tropical northern Atlantic, *Atmos. Chem. Phys*., 9, 1173–1189, doi:10.5194/acp-9-1173-2009.

Siefert, R. L., A. M. Johansen, and M. R. Hoffmann (1999), Chemical characterization of ambient aerosol collected during the southwest monsoon and intermonsoon seasons over the Arabian Sea: Labile-Fe(II) and other trace metals, *J. Geophys. Res*., 104(D3), 3511–3526, doi:10.1029/1998JD100067.

Singh, R. P., A. K. Prasad, V. K. Kayetha, and M. Kafatos (2008), Enhancement of oceanic parameters associated with dust storms using satellite data, *J. Geophys. Res*., 113, C11008, doi:10.1029/2008JC004815.

Singh, A., N. Gandhi, and R. Ramesh (2012), Contribution of atmospheric nitrogen deposition to new production in the nitrogen limited photic zone of the northern Indian Ocean, *J. Geophys. Res*., 117, C06004, doi:10.1029/2011JC007737.

Smirnov, A., B. N. Holben, T. F. Eck, O. Dubovik, and I. Slutsker (2003), Effect of wind speed on columnar aerosol optical properties at Midway Island, *J. Geophys. Res*., 108(D24), 4802, doi:10.1029/2003JD003879.

Smith, S. L. (2001), Understanding the Arabian Sea: Reflections on the 1994–1996 Arabian Sea expedition, *Deep Sea Res., Part II*, 48, 1385–1402.

Smith, S.L. *and* Madhupratap, M. (2005) Mesozooplankton of the Arabian Sea: patterns influenced by seasons, upwelling, and oxygen concentrations. *Prog. Oceanogr*. 65:214–239.

Srinivas, B., Sarin, M. and Kumar, A., (2011), Impact of anthropogenic sources on aerosol iron solubility over the Bay of Bengal and the Arabian Sea, *Biogeochem*,110 (1-3), 257-268, doi:10.1007/s10533-011-96801-1.

Sunda, W., and S. Huntsman (1995), Iron uptake and growth limitation in oceanic and coastal phytoplankton, *Mar. Chem.*, 50, 189–206.

Sunda, W. G. (1997), Control of dissolved iron concentrations in the world ocean: A comment, *Mar. Chem*., 57, 169–172.

Takeda, S., A. Kamatani, and K. Kawanobe (1995), Effects of nitrogen and iron enrichments on phytoplankton communities in the northwestern Indian Ocean, *Mar. Chem*., 50, 229–241.

Taylor S.R. and McLennan S.H. (1985), The continental crust: its composition and evolution, Blackwell (Oxford).

Vu, H.T.D., and Y. Sohrin (2013), Diverse stoichiometry of dissolved trace metals in the Indian Ocean, *Sci. Rep. 3*, p. 1745,doi:10.1038/srep01745.

Wiggert, J.D., and R.G. Murtugudde (2007), The sensitivity of the southwest monsoon phytoplankton bloom to variations in aeolian iron deposition over the Arabian Sea, *J. Geophys. Res*., Vol. 112, C05005, doi: 10.1029/2006JC003514.

Wiggert, J. D., R. R. Hood, S. W. A. Naqvi, K. H. Brink, and S. L. Smith (2009), Indian Ocean

Biogeochemical Processes and Ecological Variability, Geophysical Monograph Series Vol. 185, American Geophysical Union, 429pp.

Yu, L., and R. A. Weller (2007), Objectively analyzed air-sea heat fluxes for the global ice-free oceans (1981–2005), *Bull. Am. Meteorol. Soc*., 88, 527–539.

Zakey, A. S., F. Solmon, and F. Giorgi (2006), Development and testing of a desert dust module in a regional climate model, *Atmos. Chem. Phys*., 6, 1749–1792.

Zhu, A., V. Ramanathan, F. Li, and D. Kim (2007), Dust plumes over the Pacific, Indian, and Atlantic oceans: Climatology and radiative impact, *J. Geophys. Res*., *112*, D16208, doi:10.1029/2007JD008427.

Zhuang, G., Z. Yi, R. A. Duce, *and* P. R. Brown *(*1992), Chemistry of iron in marine aerosols, *Global Biogeochem. Cycles*, 6*(2),* 161–173, doi:10.1029/92GB00756.

Table 1. Estimated dust deposition in the CAS following dust storms and the possible amount of nutrients that can be derived from dust.

Episode number	* Dust storm detected by satellite	Total dust deposition (mg/m^2)	Wet deposition (%)	MLD during dust storm (m)	NO_3 supplied (nM)	PO_4 supplied (pM)	‡DFe upplied (1%)	‡DFe supplied (10%)	‡ DFe supplied (50%)
E1	12-14 Dec 2003	50	38.0	49	0.32	3.2	0.01	0.10	0.34
E2	09 Feb 2004	5	10.0	59	0.03	0.3	-----	0.01	0.03
E3	04Jan 2007	23	72.0	58	0.13	1.3	-----	0.03	0.13
E4	01-03 Dec 2007	9	30.0	35	0.08	0.8	-----	0.02	0.07
E5	06-07 Jan 2008	5	8.0	50	0.03	0.3	-----	0.01	0.03
E6	02-05 Feb 2008	161	25.0	56	0.91	9.1	0.02	0.20	1.0
E7	22-23 Feb 2008	12	0.4	45	0.08	0.8	-----	0.02	0.1
E8	14-15 Mar 2008	12	0.1	22	0.17	1.7	------	0.04	0.18

* The episode dates are given based on satellite detection of the dust storms. It may take few days for the plume to reach CAS. ‡ Unit of DFe is in nmol/l (nM) obtained after considering the dust deposition normalized within the mixed layer. DFe (1%), (10%) and (50%) refers to the fraction of Fe in the dust that is soluble. The DFe values that are less than 0.01 are indicated by -----.

Table 2. Nutrient requirements for the observed surface Chl *a* enhancements in CAS.

Episode Number	Period of the bloom	Maximum Chl *a* during bloom (mg/m^3)	MLD during bloom (m)	Total N (C:N:P=106:16:1)	PO_4	DFe (Fe:C=7.5)	DFe (Fe:C=12.8)	DFe (Fe:C=33.9)
E1	28 Dec 2003-07 Feb 2004	1.40	56 (MP)	3.29	0.20	0.16	0.28	0.74
E2	17 Feb -08 Mar 2004	1.57	36 (SP)	3.69	0.23	0.18	0.31	0.82
E3	30 Jan -04 Feb 2007	0.92	42 (SP)	2.16	0.13	0.11	0.18	0.48
E4	10-24 Dec 2007	1.20	38 (DP)	2.82	0.18	0.14	0.23	0.63
E5	15-17 Jan 2008	0.72	52 (DP)	1.69	0.11	0.08	0.14	0.38
E6	20-22 Feb 2008	1.70	32 (SP)	3.99	0.25	0.20	0.34	0.89
E7	29 Feb-11 Mar 2008	2.14	28 (SP)	5.03	0.31	0.25	0.42	1.12
E8	17-19 Mar 2008	0.79	22 (NC)	1.85	0.12	0.09	0.16	0.42

Units: N and PO_4 are expressed in µM; Fe/C, (µmol/mol) and DFe in nM . Note the calculated DFe value in CAS is ~0.2 nM. The cell Fe/ C quota in the phytoplankton increases with the increase in external DFe availability. MP refers to mature phase of convection-driven mixed layer deepening, SP= shallowing phase, DP=Deepening phase, NC=No convection.

Figure Captions

Figure 1. (a) Time series plots of monthly aerosol optical depth τ (red filled square) and dust optical depth τ_{du} (blue line) for the Arabian Sea (AS). (b) Shading shows distribution of correlation coefficient between τ_{du} and chlorophyll *a* (Chl *a*) concentration (mg/m^3) for the winter monsoons (WM) over the AS. The thick white contours indicate the region having coefficient of correlation between τ_{du} and Chl *a* greater than 0.5. The black contours show the distribution of the correlation coefficient between τ_{du} and Fluorescence Line Height (FLH). The green box outlines the region central Arabian Sea (CAS) which is considered for studying the effect of episodic dust storms on phytoplankton biomass (see Section 3.3).The dashed black box demarcates north AS (NAS) (see the text). (c) Climatology of Chl *a* concentration over the AS constructed over the WMs of 2002-2003 to 2010-2011. The contours indicate the climatological distribution of τ_{du} and the vectors represent the current in m/s during the same period. (d) The blue squares are the mixed layer depth (MLD) calculated from Argo data to which a third order polynomial curve was fitted for NAS and a second order polynomial curve was fitted for CAS as indicated by the blue curves. Daily climatology of modeled MLD is shown by the black lines for NAS (upper panel) and CAS (lower panel).

Figure 2. (a) Shading shows the climatological distribution of surface nitrate during the winter monsoon time and the contours indicate the sea surface temperature from World Ocean Atlas 2009 (WOA09) (b) Shading indicates north-south gradient in nitrate values obtained from JGOFS measurements during January. Superimposed are the north-south variations in temperature from WOA09.

Figure 3. Simulated dust deposition (mg/m^2) for the 02nd to 05th February, 2008 dust storm using RegCM4 model. The total deposition is for the period 01st to 07th February, 2008. The black contours indicate the difference between τ_{du} sensed from MODIS/Aqua and model simulation. Continuous contours indicate positive difference and dashed contours indicate negative difference. Filled circles indicate the amount of dust deposition (mg/m^2/day) that has been calculated from the sediment traps from *Clemens* [1998].

Figure 4. Time series of 3-day averaged chlorophyll *a* (Chl *a*) concentration (mg/m^3) and mixed layer depth (MLD) in central Arabian Sea (CAS) region for the winter monsoon of 2002-2003 to 2010-2011. The green dashed line shows the 3-day Chl *a* climatology and the vertical lines represent their 2 standard deviations; the red squares are the Chl *a* concentrations for each corresponding year; the blue line is the MLD; the black squares indicate the windows when dust storms were observed by satellite around CAS and the hollow black rectangles indicate the cases of Chl *a* enhancement when Chl *a* exceeded 2 SD level. The numbers on the top of the rectangles indicate the episode numbers which are referred in the text as E1, E2 and so on.

Figure 5. Schematic representation of the time evolution of mixed layer in the Arabian Sea during the winter monsoon and its association with the episodic chlorophyll enhancements. E1 to E8 indicates the numbers of the episodes of chlorophyll enhancements.

Figure 6. Matrix showing the possible scenarios when observed phytoplankton bloom can be ascribed to be driven by dust depositions and oceanic supply of DFe under varying Fe dissolution threshold and Fe/C ratio. The episodes listed in black are entirely supported by oceanic DFe. The episodes listed in red need an atmospheric source of DFe. The episodes that have not been listed are the ones which cannot be supported even with the atmospheric and oceanic sources of DFe taken together.

Figure 7. Schematic diagram showing the mechanism leading to chlorophyll *a* enhancement in the central Arabian Sea following dust storms during the winter monsoons (see text for explanation).

Figure 8. Mean winter monsoon time chlorophyll *a* concentration (mg/m^3) for (a) heavy dust years (2003-2004, 2006-2007 and 2007-2008) and (b) less dust years (2002-2003, 2004-2005, 2005-2006, 2008-2009,2009-2010 and 2010-2011) within central Arabian Sea.

Fs01. Simulated total dust deposition (mg/m^2) using RegCM4 model for the dust storms following which chlorophyll enhancements were noticed. The black contours indicate the difference between τ_{du} sensed from MODIS/Aqua and model simulation. Continuous contours indicate positive difference and dashed contours indicate negative difference.

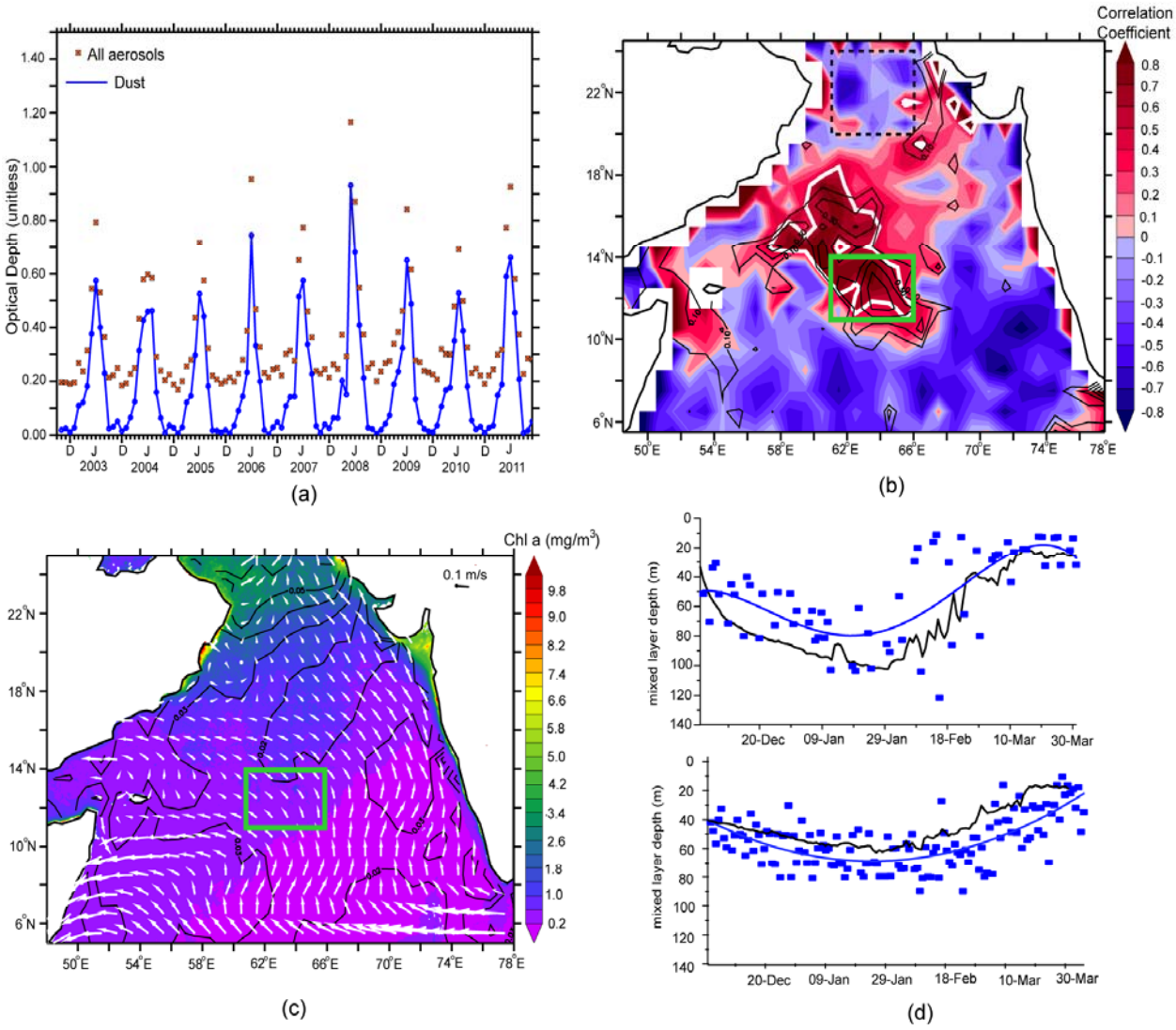

Figure 1. (a) Time series plots of monthly aerosol optical depth τ(red filled square) and dust optical depth τ_{du} (blue line) for the Arabian Sea (AS). (b) Shading shows distribution of correlation coefficient between τ_{du} and chlorophyll *a* (Chl *a*) concentration (mg/m^3) for the winter monsoons (WM) over the AS. The thick white contours indicate the region having coefficient of correlation between τ_{du} and Chl *a* greater than 0.5. The black contours show the distribution of the correlation coefficient between τ_{du} and Fluorescence Line Height (FLH). The green box outlines the region central Arabian Sea (CAS) which is considered for studying the effect of episodic dust storms on phytoplankton biomass (see Section 3.3).The dashed black box demarcates north AS (NAS) (see the text). (c) Climatology of Chl *a* concentration over the AS constructed over the WMs of 2002-2003 to 2010-2011. The contours indicate the climatological distribution of τ_{du} and the vectors represent the current in m/s during the same period. (d) The blue squares are the mixed layer depth (MLD) calculated from Argo data to which a third order polynomial curve was fitted for NAS and a second order polynomial curve was fitted for CAS as indicated by the blue curves. Daily climatology of modeled MLD is shown by the black lines for NAS (upper panel) and CAS (lower panel).

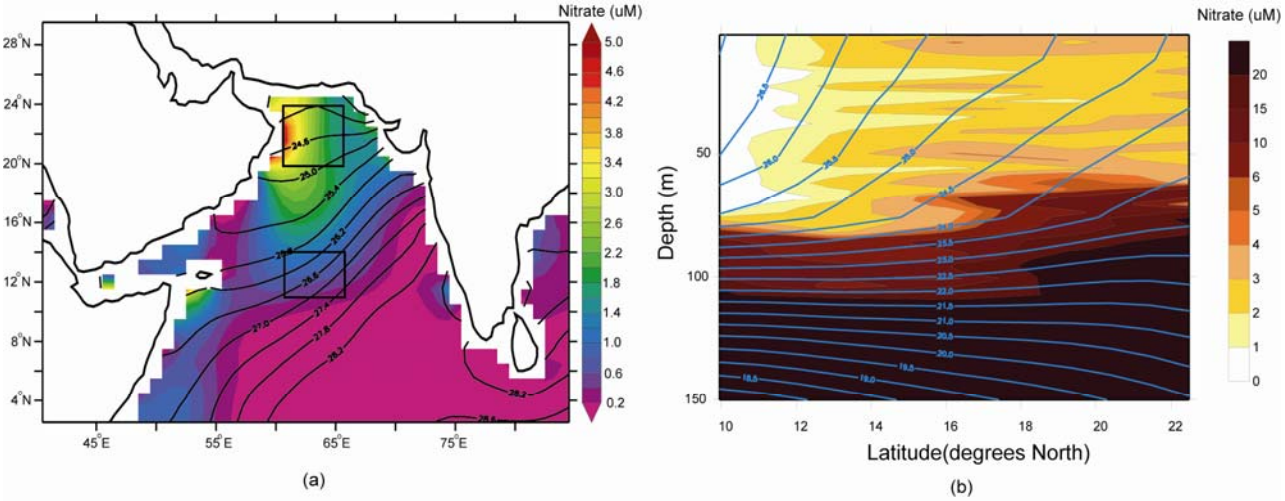

Figure 2. (a) Shading shows the climatological distribution of surface nitrate during the winter monsoon time and the contours indicate the sea surface temperature from World Ocean Atlas 2009 (WOA09) (b) Shading indicates north-south gradient in nitrate values obtained from JGOFS measurements during January. Superimposed are the north-south variations in temperature from WOA09.

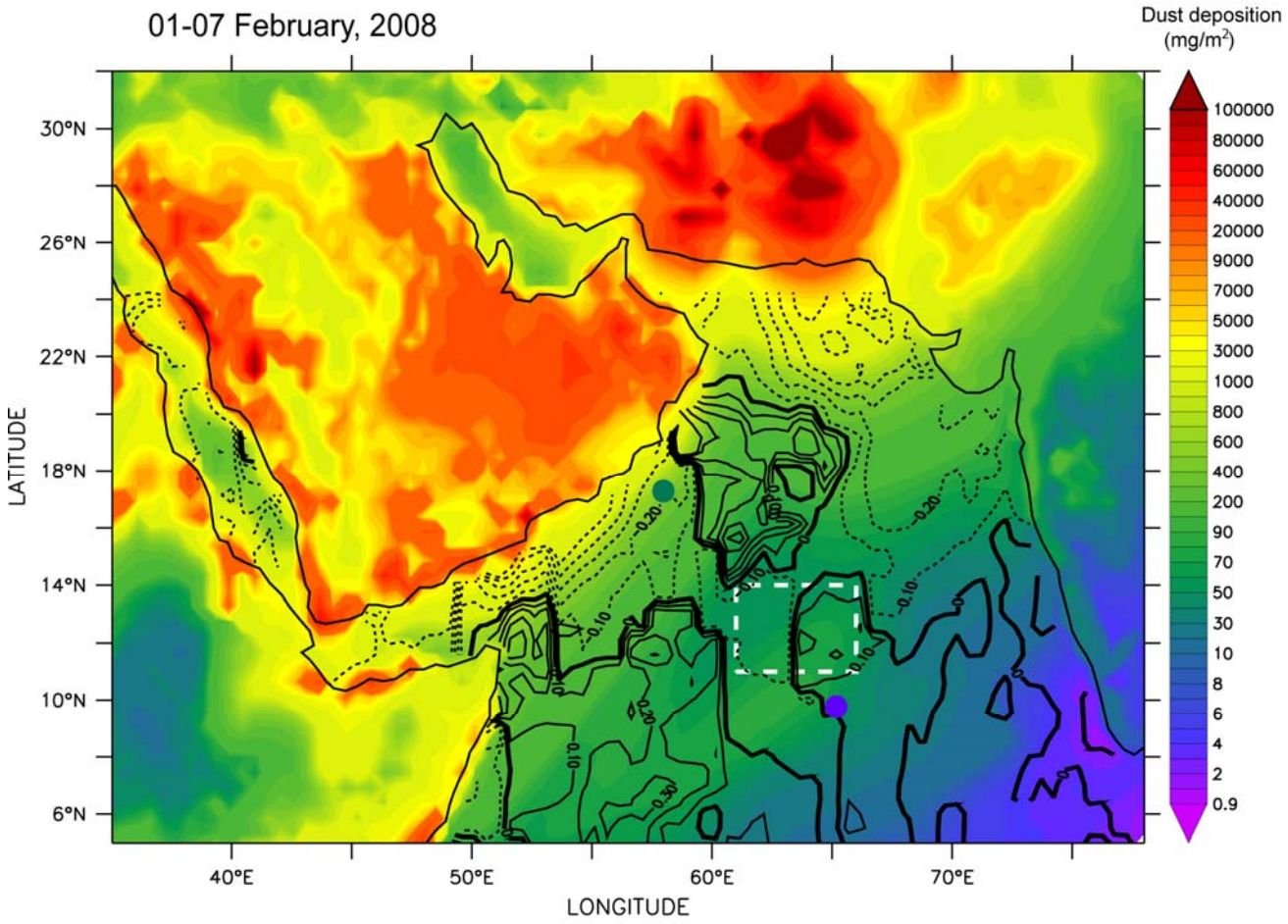

Figure 3. Simulated dust deposition (mg/m^2) for the 02nd to 05th February, 2008 dust storm using RegCM4 model. The total deposition is for the period 01st to 07th February, 2008. The black contours indicate the difference between τ_{du} sensed from MODIS/Aqua and model simulation. Continuous contours indicate positive difference and dashed contours indicate negative difference. The circular symbols indicate the amount of dust deposition (mg/m^2/day) that has been calculated from the sediment traps from Clemens [1988].

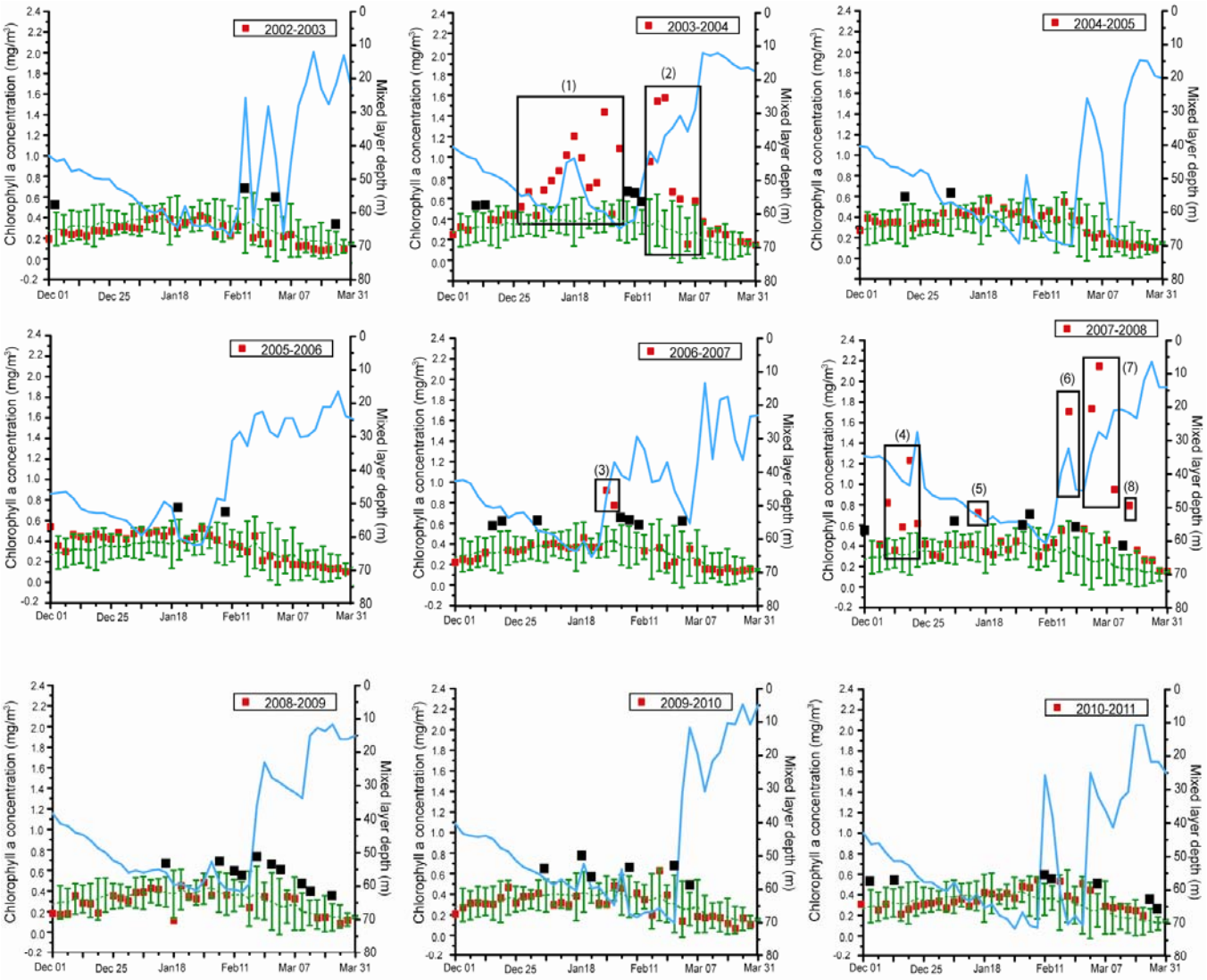

Figure 4. Time series of 3-day averaged chlorophyll *a* (Chl *a*) concentration (mg/m^3) and mixed layer depth (MLD) in central Arabian Sea (CAS) region for the winter monsoon of 2002-2003 to 2010-2011. The green dashed line shows the 3-day Chl *a* climatology and the vertical lines represent their 2 standard deviations; the red squares are the Chl *a* concentrations for each corresponding year; the blue line is the MLD; the black squares indicate the windows when dust storms were observed by satellite around CAS and the hollow black rectangles indicate the cases of Chl *a* enhancement when Chl *a* exceeded 2 SD level. The numbers on the top of the rectangles indicate the episode numbers which are referred in the text as E1, E2 and so on.

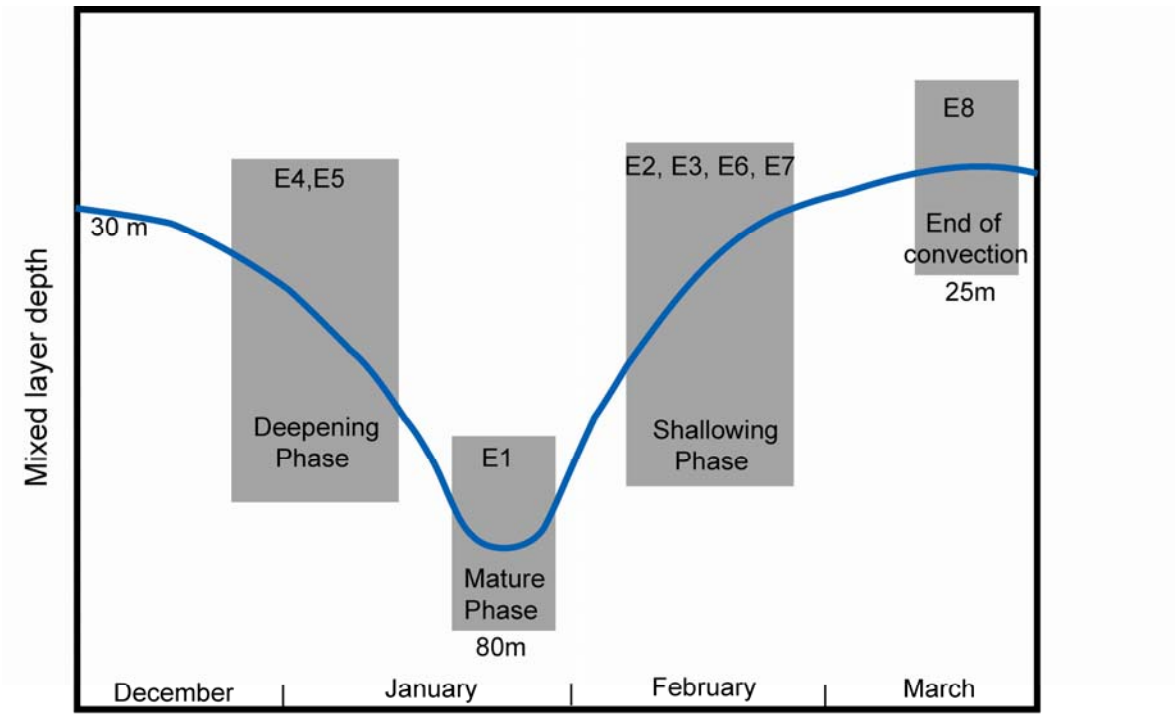

Figure 5. Schematic representation of the time evolution of mixed layer in the Arabian Sea during the winter monsoon and its association with the episodic chlorophyll enhancements. E1 to E8 indicates the numbers of the episodes of chlorophyll enhancements.

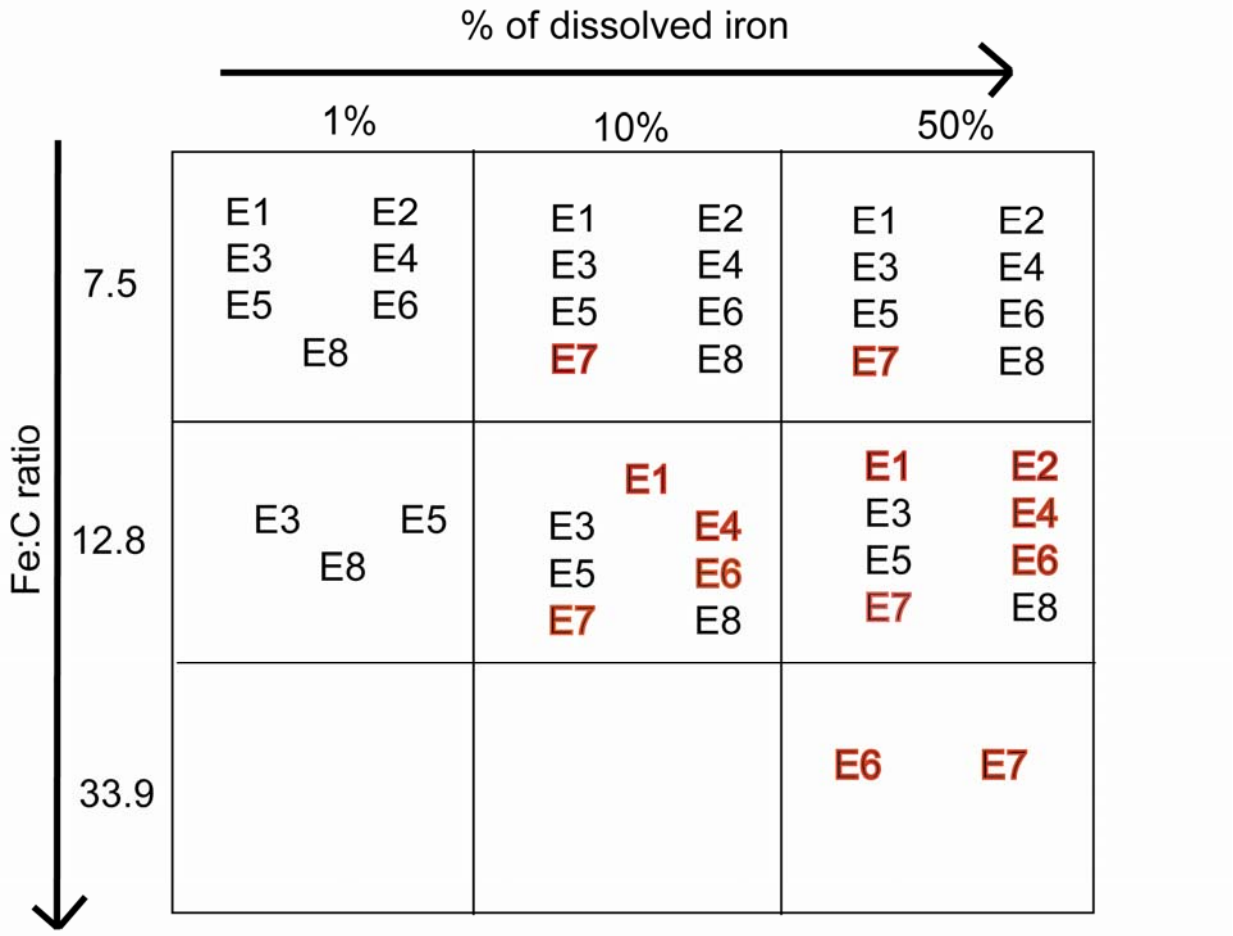

Figure 6. Matrix showing the possible scenarios when observed phytoplankton bloom can be ascribed to be driven by dust depositions and oceanic supply of DFe under varying Fe dissolution threshold and Fe/C ratio. The episodes listed in black are entirely supported by oceanic DFe. The episodes listed in red need an atmospheric source of DFe. The episodes that have not been listed are the ones which cannot be supported even with the atmospheric and oceanic sources of DFe taken together.

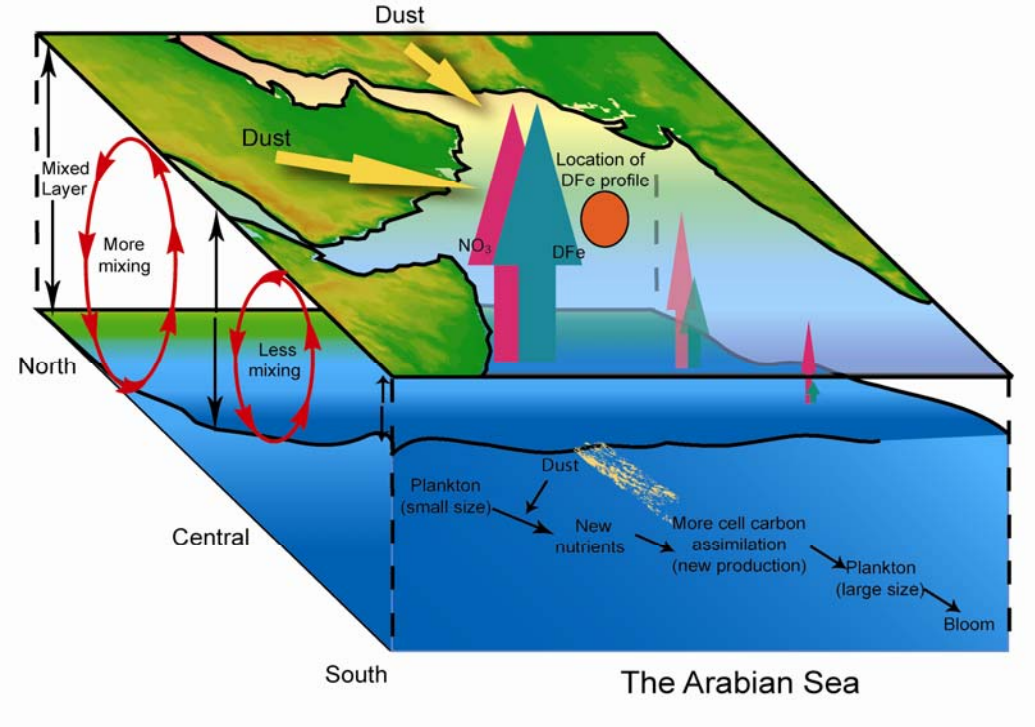

Figure 7. Schematic diagram showing the mechanism leading to chlorophyll *a* enhancement in the central Arabian Sea following dust storms during the winter monsoons (see text for explanation).

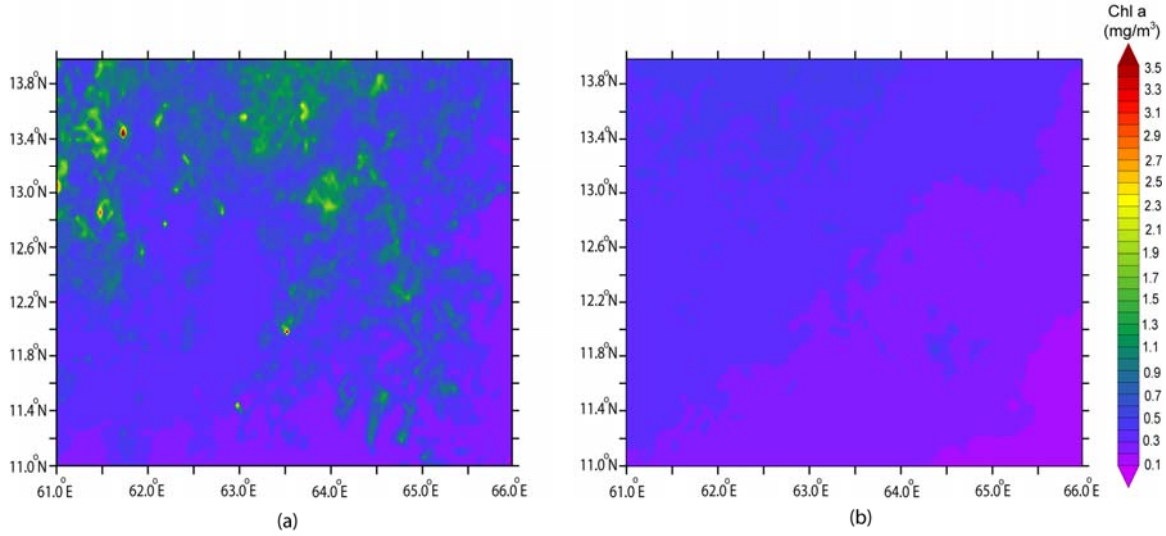

Figure 8. Mean winter monsoon time chlorophyll *a* concentration (mg/m^3) for (a) heavy dust years (2003-2004, 2006-2007 and 2007-2008) and (b) less dust years (2002-2003, 2004-2005, 2005-2006,2008-2009,2009-2010 and 2010-2011) within central Arabian Sea.

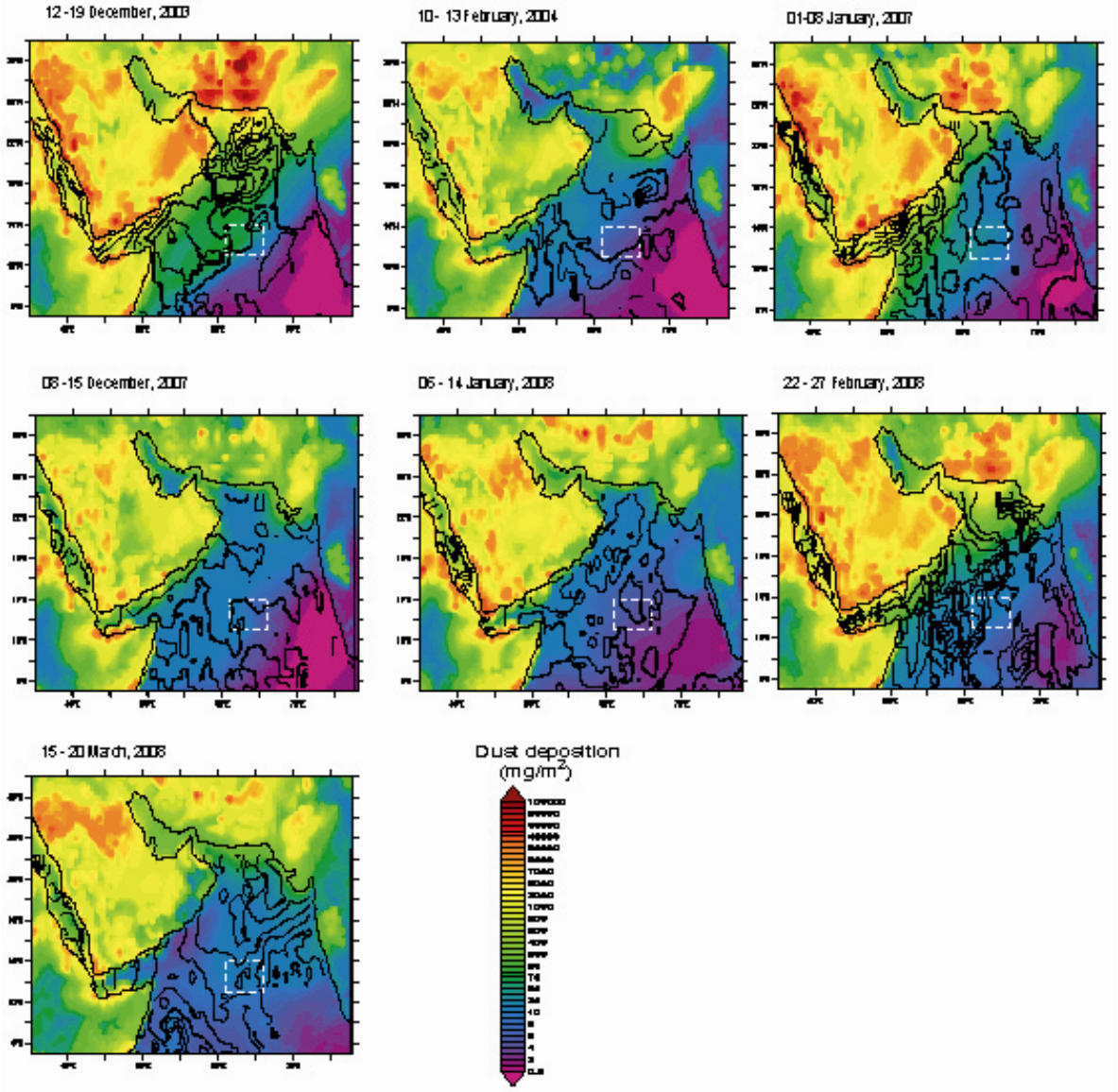

Fs01. Simulated total dust deposition (mg/m^2) using RegCM4 model for the dust storms following which chlorophyll enhancements were noticed. The black contours indicate the difference between τ_{du} sensed from MODIS/Aqua and model simulation. Continuous contours indicate positive difference and dashed contour indicate negative difference.